Malaysian Journal of Chemistry, 2024, Vol. 26(4), 206-220

Exploring the Photonic System via Investigating Acidic and Normal Photoetching Behaviour to Improve Dye Photodegradation on TiO_2/ENR/PVC Immobilization

Siti Raihan Hamzah, Muhammad Afiq Rosli, Nur Aien Muhamad, Nadiah Sabihah Natar, Nureel Imanina Abdul Ghani, Mohammad Saifulddin Azami, Mohd Azlan Mohd Ishak, Razif Nordin[1], Khudzir Ismail and Wan Izhan Nawawi*

Faculty of Applied Sciences, Universiti Teknologi MARA (UiTM), Cawangan Perlis, Kampus Arau, 02600 Arau, Perlis, Malaysia

*Corresponding author (e-mail: wi_nawawi@uitm.edu.my)

Titanium dioxide with a polymer binder (TiO_2/ENR/PVC) was successfully immobilized on a glass substrate by the dip coating technique. The comparison between immobilized photocatalysts with normal photoetching (NP) and acid photoetching (AP) treatments was based on photocatalytic performance and advanced instrumental characterization. A 65 W compact fluorescent lamp and Reactive Red 4 (RR4) dye solution were used to measure the photocatalytic activity for 18 cycles (1 cycle = 10 hours). All the samples were characterized before and after both treatments by FESEM, 3D profilometer, XRD, FTIR and PL to ascertain the surface interactions of the immobilized TiO_2 in the presence of hydrochloric acid (HCl), and reaction pathways after photoetching treatment were proposed. The AP sample showed the highest photocatalytic performance with a 0.13 min^{-1} pseudo 1st order rate constant (k) value, in comparison to the NP sample. Ring-opening and crosslinking reactions after the acid photoetching treatment enhanced photocatalytic activity. Deterioration in the AP and NP samples after the 12th cycle was due to the percolation of the polymer binder on the surface of the samples. Hence, normal and acid photoetching treatments enhanced photocatalytic activity and enabled the immobilized sample to be reused for 18 cycles due to the ring-opening and crosslinking reactions that occurred during these treatments.

Keywords: Titanium dioxide; polymer semiconductor; photoetching; dye photodegradation; immobilized photocatalyst

Received: June 2024; Accepted: July 2024

The textile industry encounters considerable difficulties in effectively handling its wastewater throughout the textile finishing process, which involves a range of dyes and organic substances. The presence of these pollutants poses a threat to aquatic organisms by disturbing their natural equilibrium, primarily because dyes are not easily broken down by natural processes [1-3]. Photocatalysis has emerged as a promising approach towards advanced oxidation processes for dye pollution degradation. Titanium dioxide (TiO_2) is a widely preferred semiconductor photocatalyst due to its cost-effectiveness, stability, and non-toxic nature, making it stand out among other semiconductors [4-6]. Historically, photocatalysis has been carried out in a slurry system, resulting in outstanding efficiency. Nevertheless, this approach requires costly and unfeasible filtering throughout the subsequent treatment [7-10]. In order to address this constraint, an immobilization system has been implemented, which removes the necessity for post-treatment filtering. This immobilization technique provides multiple benefits, such as convenience, reusability, and recyclability [11-13].

There are several ways available to immobilize TiO_2 on a solid substrate, including physical deposition [14], electrodeposition [15], the sol-gel approach [16], chemical vapour deposition [17], and electrophoretic deposition [18]. The application of immobilized TiO_2 has received attention as it renders a post-treatment process unnecessary. However, the limited surface area of TiO_2 is a contributing element to its lower photocatalytic efficiency [19]. Chen et al. [20] stated that it is crucial to optimize the availability of the active surface area in order to get better photocatalytic activity. This is because it improves the absorption of organic compounds. Consequently, researchers have investigated methods to enhance the surface area of immobilized TiO_2, such as by adding nanoparticles or forming a porous structure [21-22]. The selection of a binder may also have significant effects on the immobilization procedure and the resulting properties of the TiO_2 film. Specific binders may improve the adherence of the TiO_2 film to the substrate, thus facilitating superior photocatalytic activity. Hence, it is important to precisely evaluate both the immobilization techniques and the binder in order to

produce a TiO_2 film with the required properties and effectiveness.

Utilizing a polymer binder in immobilized TiO_2 is a widely used method to improve its adhesion, temperature resistance, and durability against pollutants [5, 14, 23-24]. Specific categories of polymers have been found to enhance the photocatalytic efficiency of TiO_2 when used as a binder. A comprehensive study has been conducted on the immobilization of TiO_2 using polymer binders since its initial discovery by Akira Fujishima and Kenichi Honda in 1972 [25]. Since then, various methods have been explored to immobilize TiO_2 using different polymer alcohol (PVA) [27], polyacrylic acid (PAA) [28-29], polyethylene glycol (PEG) [24, 27, 30], polyvinylpyrrolidone (PVP) [23, 31], polyethyleneimine (PEI) [32], polydopamine (PDA) [33], chitosan [34], gelatine [35], and polyurethane (PU) [36]. Composite binders such as ethylene vinyl acetate (EVA) [37] and ethylene vinyl alcohol (EVOH) [38] have also been investigated for various uses. Recent research has shown that the combination of epoxidized natural rubber (ENR)/polyvinyl alcohol (PVC) is a highly effective binder for generating photocatalytic TiO_2 films with good adhesion and durability properties [39], making it a potential option for diverse applications. Nevertheless, it is important to acknowledge that an elevated polymer concentration may decrease photocatalytic activity by reducing the interactions between TiO_2 and the surfactant.

To address this problem, a photoetching technique has been implemented to eliminate organic and inorganic substances from the surface of the photocatalyst. A comprehensive study was carried out to study the effects of this treatment on the surface of immobilized TiO_2/ENR/PVC. It was found that the ENR-50 additive could be effectively eliminated by subjecting it to a 5-hour photoetching process, resulting in the formation of a porous surface [8, 40]. It was hypothesized that PVC undergoes conversion to polyene during the photoetching procedure, resulting in an increase in photocatalytic activity [41]. Moreover, crosslinking reactions between ENR and PVC help to attach TiO_2 to the glass substrate. The photoetching procedure may also eliminate ENR-50 from the attached TiO_2, which reduces its ability to stick to surfaces. Hamzah et al. [42] have reported that a ring-opening reaction may occur in ENR-50 under mild acid conditions. Consequently, the presence of acid is expected to enhance the ENR-50 ring-opening reaction, resulting in significant crosslinking reactions. In addition, the radicals produced by the ENR-50 ring-opening may increase photocatalytic activity by reacting with the Reactive Red 4 (RR4) dye during the photodegradation process. However, there have been few reported studies focusing on acid photoetching treatment of photocatalysts for dye photodegradation.

This work aims to compare the effects of acid and normal photoetching treatments on immobilized TiO_2/ENR/PVC for the photodegradation of RR4 dye. A detailed reaction pathway for the treatment is proposed based on FTIR analysis. These results should contribute to a more comprehensive understanding of how TiO_2 immobilized with polymer binders enhances photocatalytic activity.

EXPERIMENTAL

Chemicals and Materials

The experimental setup involved the utilization of commercial Degussa P-25 TiO_2 nano powder, consisting of 80 % anatase and 20 % rutile (Acros Organics, Geel, Belgium). Two polymeric binders, ENR-50 (Kumpulan Guthrie, Kuala Lumpur, Malaysia) and PVC (Petrochemicals (M), Johor, Malaysia) were used to immobilize TiO_2. The solvents used (R&M Chemicals, Selangor, Malaysia) in this study were toluene (C_7H_8, 99.5 %) and dichloromethane (DCM, CH_2Cl_2, 99.5 %). To simulate real-world conditions, Reactive Red 4 (RR4) dye (Sigma-Aldrich (M), Petaling Jaya, Malaysia), also known as Cibacron Brilliant Red, with a dye content of 50 % was chosen as the model pollutant due to its widespread use in various industries. Ultra-pure water with a purity of 18.2 MW cm^{-1} was used for solution preparation and dilution throughout the study. The ENR-50 reflux process was conducted using a stirring heating mantle (Fisher Scientific, Gelugor, Penang). The formulation of the immobilized photocatalyst (TiO_2/ENR/PVC) was homogenized using a Crest Ultrasonic cleaner model 4NT-1014-6 (50–60 kHz) (Crest Systems (M), Bayan Lepas, Penang). Illumination was provided by compact household fluorescent lamps (55 W and 65 W) manufactured by Firefly Electric & Lighting Corp. in Manila, Philippines, which emitted a UV leakage irradiance of 6.0 W m^{-2}. The aeration source was produced by an aquarium pump model NS 7200 (Ace Story Aquatic, Penang, Malaysia). For the photocatalytic processes, custom-made glass cells with dimensions of 58 mm length, 10 mm width, and 80 mm height were utilized. A glass plate (47 mm × 70 mm) with a ground surface on one side served as the support material for immobilizing the TiO_2/ENR/PVC formulation.

Characterization Methods

The concentration of RR4 was determined using a DR2000 UV-visible (UV-vis) spectrophotometer (HACH, Kuala Lumpur, Malaysia). Surface morphology analysis and roughness measurement were conducted using a LEO SUPRA 50 VP field emission scanning electron microscope (FESEM) (Bruker Malaysia, Penang, Malaysia) and a PEMTRON HAWK 3D WT-250 surface profilometer (Pemtron, Seoul, South Korea). Changes in functional group absorbance peaks in the treated samples were observed by Fourier Transform infrared spectroscopy (FTIR), with a Perkin-Elmer 2000 FTIR (Perkin Elmer, Selangor, Malaysia). X-ray diffraction (XRD) analysis of the

prepared samples was performed using a Bruker D8 Advance diffractometer (Bruker, Penang, Malaysia).

Fabrication of Immobilized TiO_2/ENR/PVC

The experimental procedure used in this study was adapted from a previous study [38] with slight modifications. The ENR-50 solution was made by heating 24.8 ± 0.05 g of ENR-50 in 250 mL of toluene at a temperature range of 88–90 °C until complete dissolution and a sticky consistency were achieved. For the PVC solution, 0.8 g of PVC powder was dissolved in 35 mL of dichloromethane by sonication for 1 hour. The immobilized TiO_2 formulation was prepared by gradually adding 6.0 g of TiO_2 to the ENR-50/PVC blend in a ratio of 5:1, followed by sonication to ensure a homogeneous mixture. The TiO_2 formulation was then dip-coated onto clean glass plates using a simple method as described by Nawi et al. [39]. The coated plates were dried until a TiO_2 loading of 2 g was achieved, which typically required three rounds of dip coating.

Photoetching and Acid Photoetching Treatment of Immobilized TiO_2/ENR/PVC

The coated plates, referred to as immobilized TiO_2/ENR/PVC, underwent photoetching and acid photoetching treatments for a duration of 10 hours per cycle using a compact fluorescent lamp, as shown in Figure 1. This was done by immersing the plates in a glass cell filled with etching solution (distilled water and HCl solution, respectively) for the photoetching process, for a total of 18 cycles. The solution temperature was maintained at 25 ± 1 °C throughout the process by water continuously flowing through a water jacket. An aquarium pump was used to produce aeration in order to enhance the mass transfer of RR4 dye molecules to the surface of the immobilized TiO_2.

Dye Photodegradation

The photocatalytic degradation performance of the treated immobilized TiO_2/ENR/PVC plates during each cycle was tested using a 30 ppm RR4 dye solution in a custom-made glass cell reactor illuminated by a 55 W compact fluorescent lamp. 16 ml of RR4 dye solution was used as a model pollutant for the immobilized TiO_2/ENR/PVC under aeration and illumination for an hour. Absorbance values of the pollutant solution were taken at 15-minute intervals. The absorbance of the initial concentration and at any given time (t) were measured using a spectrophotometer, and the results were plotted against irradiation or contact time. The slope of the linear line represented the pseudo first-order rate constant, based on the Langmuir-Hinshelwood rate model.

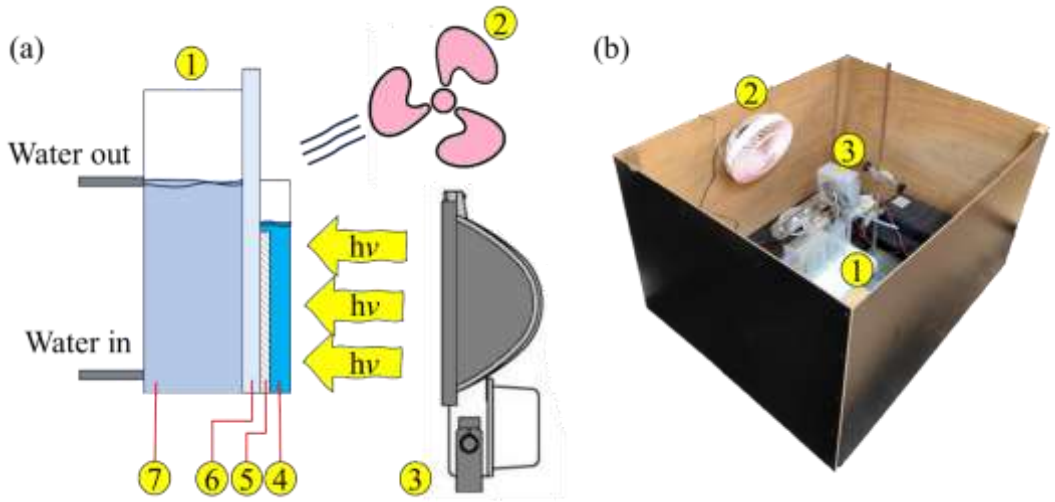

Figure 1. (a) Illustration of photoetching treatment system for the immobilized TiO_2/ENR/PVC (b) Actual experimental setup. Labels represent: (1) water jacket system; (2) fan; (3) metal halide lamp; (4) etching solution; (5) immobilized TiO_2/ENR/PVC; (6) glass substrate; (7) water flow.

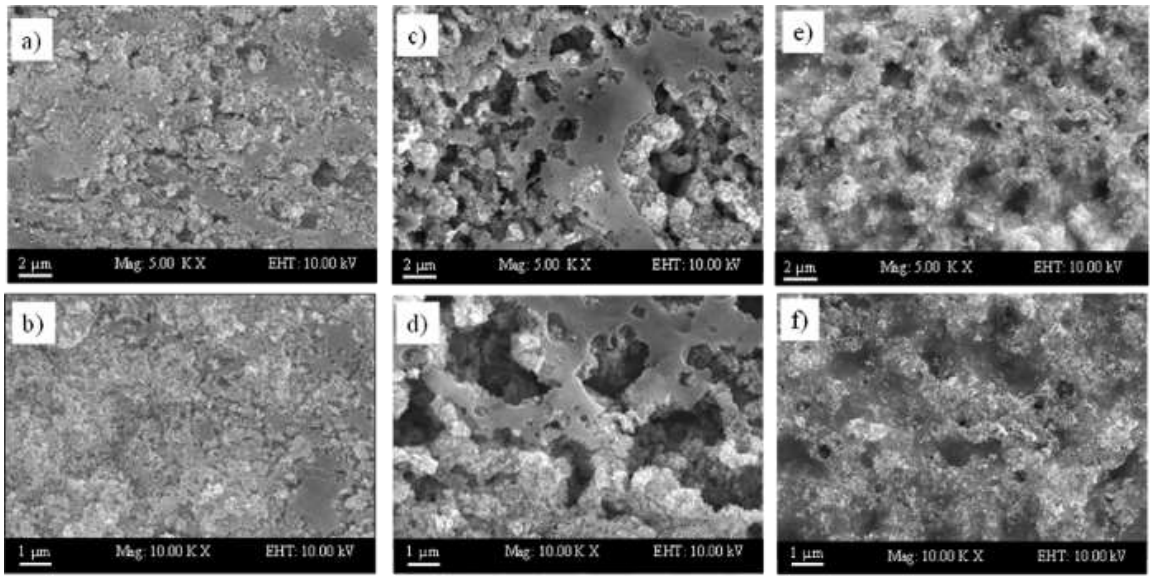

Figure 2. Field Emission Scanning Electron Microscopy (FESEM) of (a-b) WOP, (c-d) NP and (e-f) AP samples at magnifications of 5,000x and 10,000x, respectively.

RESULTS AND DISCUSSION

Surface Structural Analysis

Figure 2 displays the surface morphology of the TiO_2/ENR/PVC samples under different treatment conditions: without photoetching treatment (WOP), with normal photoetching treatment (NP), and with acid photoetching treatment (AP). The surface characteristics were observed using Field Emission Scanning Electron Microscopy (FESEM) at magnifications of 5,000x and 10,000x. FESEM images of the WOP sample are shown in Fig. 2(a, b). The images reveal a surface that appears compact and dense, suggesting the existence of a protective layer composed of ENR/PVC surrounding the TiO_2 particles. The homogeneity and density of the surface indicate robust bonds between the ENR/PVC layer and the TiO_2 particles.

In contrast, the surface of the NP sample exhibited a predominantly rough and porous texture, with several areas appearing smooth, reflecting the degradation and reduction of the fully covered ENR/PVC layer after photoetching treatment (Fig. 2(c, d)). The photoetching technique appeared to eliminate the ENR/PVC layer by means of a ring-opening crosslinking reaction, as mentioned by other researchers [5-6, 39].

The surface of the AP sample exhibited a melted appearance after undergoing the acid photoetching process (Fig. 2(e, f)). The polymer structure was exposed to 1.0 N HCl for an extended period, leading to a melted form or degradation of the ENR/PVC layer [42]. Clearly, the molten layer covered the whole TiO_2 surface, inhibiting illumination of the active sites by light. This condition is likely to result in reduced photocatalytic performance.

The surface porosity and roughness of the WOP, NP, and AP samples were analysed using a 3D optical profilometer, and the 2D surface profiles of the samples are shown in Fig. 3(a-c). The height differences of the surface in all the samples are distinguished by the colour indicator in the 2D surface profiles. The maximum height (hill) is indicated in red, while the minimum height (valley) is represented by blue. Each figure demonstrates that there were different heights on the sample surface. Fig. 3(a) displays the 2D surface profile of the coated sample (WOP) before photoetching with a hill of 109968.2 nm, which is lower than the hill of the NP sample. There are some red islands indicating the hill (173843.0 nm) and a distribution of valleys over the NP sample surface in Fig. 3(b). According to Li *et al.* [43], photoetching may enhance the specific surface area by decreasing agglomeration of the immobilized photocatalyst. Hence, the augmentation of the hill height of the NP sample may be due to the photoetching effect, as the ENR/PVC layer may be photoetched out of the immobilized sample along with TiO_2. However, the AP sample had a few dark blue islands scattered all over the sample but no red areas, with a hill height of 50320.40 nm, as shown in Fig. 3(c). This decrease in height might be due to the presence of a melted ENR/PVC layer covering the immobilized sample. In addition, the 2D surface profiles were used to obtain the surface roughness for each sample, as listed in Table 1.

The 3D surface profiles shown in Fig. 3(d-f) clearly demonstrate the cross-sections of the WOP, NP, and AP samples, respectively. Figure 3(d)

represents the surface topography of the WOP sample, which illustrates a great waviness in the hill area located at the left part of the x-axis. Figure 3(e) depicts the NP sample, which consists of a uniform distribution of high hills and valleys that show the porous surface. The valleys formed on the NP sample may be due to the loss of TiO_2 during photoetching. Photoetching of the ENR/PVC layer reduces the adhesiveness of the closest TiO_2, etching the TiO_2 out, thus producing a porous structure on the immobilized sample [39]. However, in Fig. 3(f), the AP sample displayed an even distribution of small hills which represent the sample having been covered by the ENR/PVC layer. The least porous surface of the AP sample may be due to the melted structure of the polymer after the acid photoetching treatment. Both samples' surface properties were noticeably influenced by the applied photoetching treatment in comparison to WOP.

Average roughness (R_a) and root mean square roughness (R_q) are 2D surface roughness parameters. The equations for these parameters are shown in Eqs. (1) and (2) [44]. The calculated parameters are listed in Table 1.

$$R_a = (1/N)\ \Sigma\_(J=1)\ \hat{}N\ |\ Z\_J\ | \qquad (1)$$

$$R_q = \sqrt{}\ ((1/N)\ \Sigma\_(J=1)\ \hat{}N\ |\ Z\_J\ |\ ) \qquad (2)$$

Based on Coto et al. [45], a high surface roughness and high surface area may enhance photocatalytic activity. The results presented in Table 1 provide an analysis of the surface roughness for the three samples WOP, NP, and AP. The roughness parameters, R_a and R_q, were measured for each sample. The R_a value for the WOP sample was 8,101.95 nm, indicating a relatively low roughness. Similarly, the R_q value for the WOP sample was 10,449.51 nm. On the other hand, the NP sample exhibited the highest roughness among the three samples, with an R_a value of 15,674.81 nm and an R_q value of 19,062.62 nm.

The significant difference between the surface roughness values is associated with the high porosity of the NP sample. Apparently, the AP sample demonstrated the lowest level of roughness in comparison to the other two samples, with an R_a value of 4,707.59 nm and an R_q value of 5,858.59 nm. This may be due to the melted ENR-50 that covered the TiO_2 surface, leading to low photocatalytic activity. These findings shed light on the surface characteristics and roughness of the different samples, highlighting the impact of porosity and the presence of ENR-50 on their surface properties.

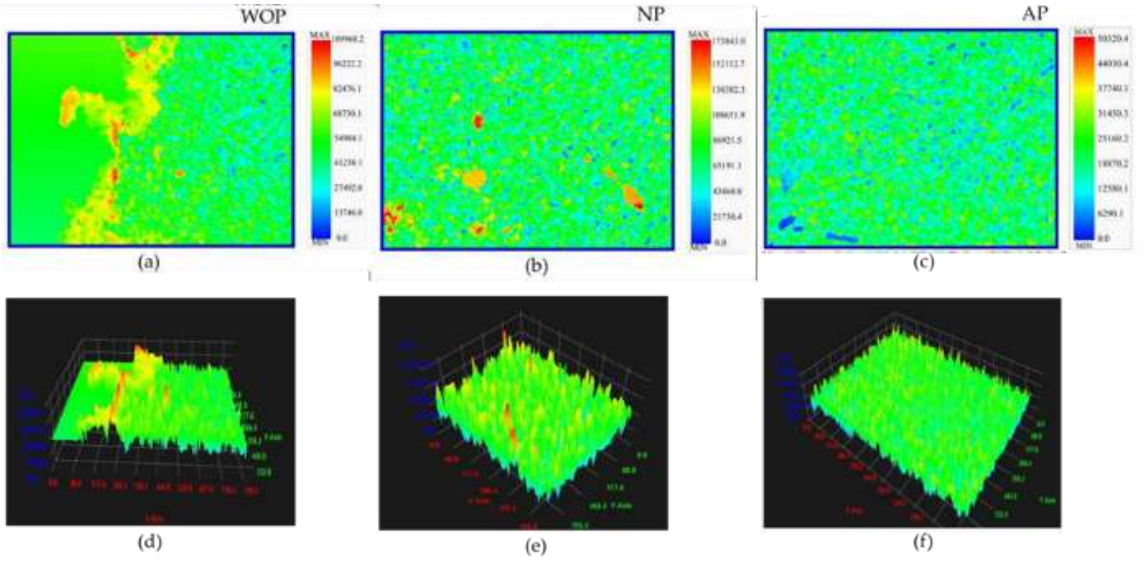

Figure 3. (a-c) 2D surface profiles and (d-f) 3D surface profiles of the WOP, NP, and AP samples, respectively.

Table 1. The average roughness (*Ra*) and familiar root mean square roughness (*Rq*) for the WOP, NP and AP samples.

Sample	Ra values (nm)	Rq values (nm)
WOP	8101.95	10449.51
NP	15674.81	19062.62
AP	4707.59	5858.59

Nitrogen (N_2) adsorption analysis was conducted to assess the specific surface area, pore diameter, and pore volume distribution of the immobilized TiO_2/ENR/PVC samples. The results of the N_2 adsorption isotherms for both NP and AP samples are depicted in Figure 4(a). It is evident that both scenarios exhibited a type II isotherm, as per the IUPAC classification, which signifies adsorption-desorption processes typically on non-porous materials as mentioned by Vittoni et al. [46]. Interestingly, the isotherm of the NP sample showed a slightly higher nitrogen adsorption compared to the AP sample, with a surface area value of 28.605 m^2/g for NP and 21.283 m^2/g for AP. This phenomenon could be attributed to the presence of larger pore diameters and increased surface area, as noted by Ambroz and colleagues. These findings align with the observations from the SEM images, indicating that the NP sample exhibited a higher pore count than the AP sample.

XRD Analysis

X-ray diffraction (XRD) analysis of the WOP, NP, and AP samples was performed using a Bruker D8 advance diffractometer in reflection mode with Cu-Kα radiation. The diffracted beam monochromator was utilized in step scan mode, with a step size of 0.075° (2θ) and a duration of 4 seconds per step. The XRD patterns of the samples are shown in Fig. 4(b).

The peaks observed in the NP sample and commercialized Degussa P25-TiO_2 were identified as anatase (JCPDS Card No: 21-1272). Commercialized Degussa P25-TiO_2 contains more than 70 % anatase, along with a minor amount of rutile [47]. Moreover, the fine particle grain size of anatase which has a larger band gap (3.2 eV) is more favourable to photoactivity in comparison to rutile, which has a small band gap (3.0 eV) [48].

The positions of 2θ, ranging from 25.31° to 70.30°, corresponded to various planes with Miller indices such as (101), (103), (004), (112), (200), (105), (211), (116), (220), and (215). Strong diffraction peaks were observed at 25.31° and 48.04°, confirming the presence of anatase in the samples. The higher intensities of these peaks were attributed to the etching of the polymer, which exposed more TiO_2 crystals to the X-ray probe. This is supported by the sharper peaks observed in the NP, AP, and P25-TiO_2 samples in comparison to the WOP sample. The WOP sample contained the most polymer binder, which hindered the crystalline structure of TiO_2.

These findings further support the concept that the ENR component of the NP and AP samples had been photoetched out of the immobilized TiO_2/ENR/PVC. Previous researchers [39-40, 49] have also mentioned this phenomenon. Consequently, the adhesiveness of the immobilized TiO_2/ENR/PVC may be compromised due to the reduction of ENR content in the samples, leading to its potential peeling off of the glass substrate.

Possible Reaction Mechanism Pathways

Figure 5 shows the FTIR spectra of the TiO_2 samples, including AP, WOP, NP, and commercialized Degussa P-25. The presence of PVC was indicated by peaks at 1251, 1332, and 1432 cm^{-1} which were assigned to the C-H stretching and vibrations of the CH-Cl groups, while the ENR-50 compound was indicated by the peak at 1432 cm^{-1} (C-H bending vibrations) [39-40, 49]. The reduction in peak intensities at 1251 and 1432 cm^{-1} reflects the destruction of CH_2Cl deformation in PVC and the reduction of ENR-50 due to ring-opening and the crosslinking reaction between ENR-50 and PVC during the normal photoetching treatment.

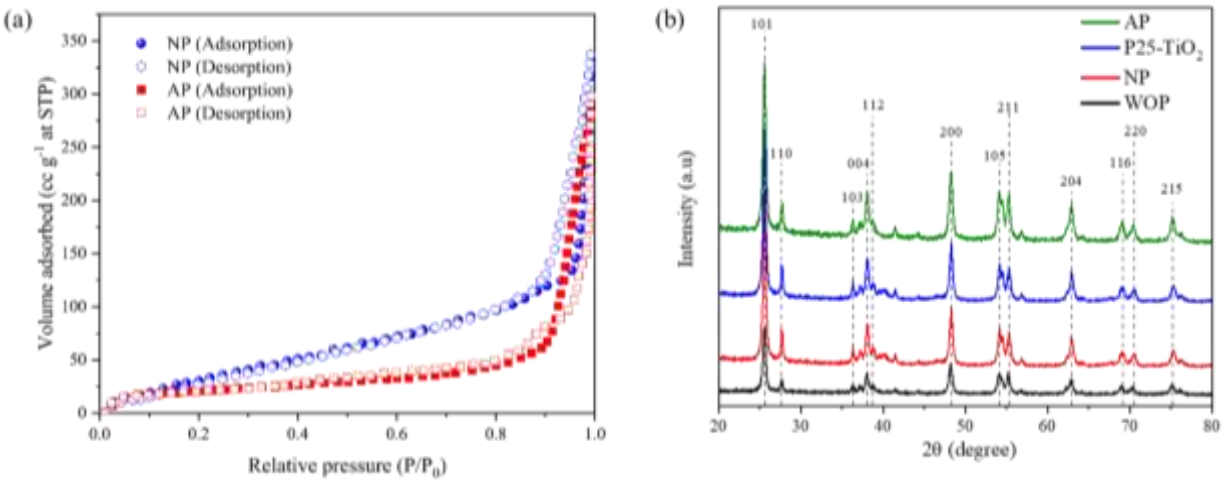

Figure 4. (a) Nitrogen adsorption and desorption isotherms of the NP and AP samples, respectively, and (b) X-ray diffraction patterns of P25-TiO_2, WOP, NP and AP.

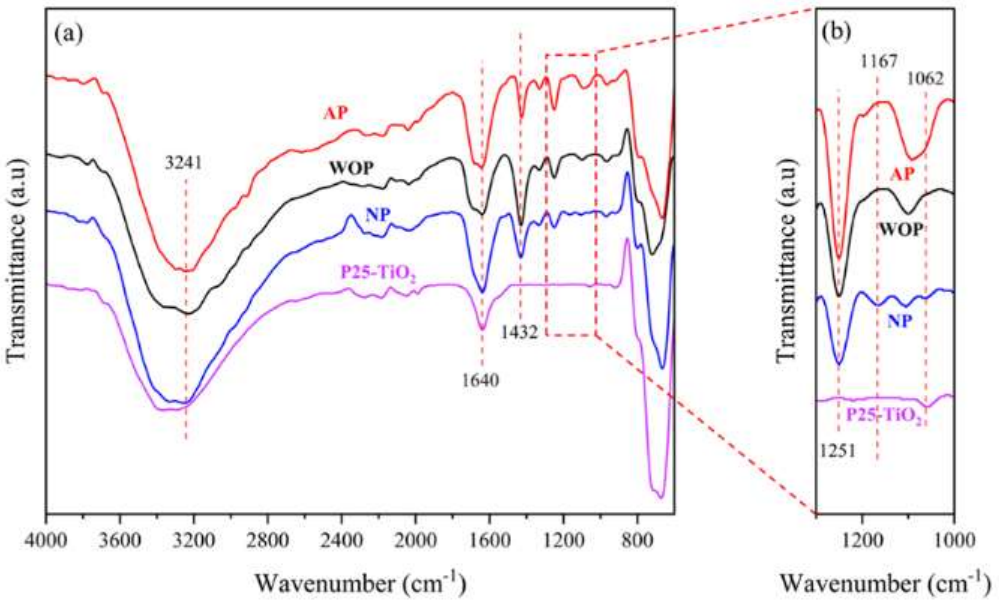

Figure 5. Comparison of Fourier Transform infrared (FTIR) spectra of WOP, NP, AP and P25-TiO_2.

The formation of aliphatic ether due to the crosslinking reaction was confirmed by two new peaks indicating C-O bonds in the NP spectrum at 1167 and 1062 cm^{-1}, despite porosity formation due to ENR being leached out. Crosslinking may contribute to maintaining the adhesive properties of the sample on the glass substrate, as stated by Nawi et. al. [39] and Ramlee et. al. [49]. The remaining ENR is involved in a crosslinking reaction, as shown in the proposed reaction mechanism in Fig. 6.

Alternatively, the PVC may be converted into a polyene precursor, which serves as a photosensitizer, enhancing TiO_2's photocatalytic activity [39]. However, the AP sample showed a shoulder peak at 1062 cm^{-1} and higher intensity peaks at 1097 cm^{-1} and 1255 cm^{-1} among all the samples. The shoulder peak proves that there was a crosslinking reaction, as the peak of 1062 cm^{-1} represents C-O bonds in the ether product, while the 1097 cm^{-1} and 1255 cm^{-1} peaks, respectively, indicate asymmetric and symmetric C-O-C stretching vibrations in the epoxide ring of ENR. The AP spectrum also indicates ENR ring-opening as the peak intensity at 1432 cm^{-1} was reduced in comparison to the sample without any treatment (WOP).

For normal photoetching treatment, the probable reaction mechanisms consisting of ring-opening and crosslinking reactions are displayed in Fig. 6. ENR-50 is composed of a highly strained oxirane ring that is susceptible to opening under mild conditions. This process leads to the formation of radicals during the ring-opening reaction. The photoetching process alters the structure of the oxirane ring in ENR-50 through the ring-opening reaction, resulting in one of two crosslinking reactions illustrated in Figure 6 (1) and (2). In these reactions, the opened ring of an ENR-50 molecule reacts with PVC or another ENR-50 molecule to produce an ether crosslinked product. These products may enhance the durability and adhesiveness of immobilized TiO_2, as mentioned by previous researchers [39-40, 49]. Moreover, it is believed that the radicals formed by the ring-opening reaction react with the RR4 dye during the photocatalytic degradation process. As light penetrates the immobilized TiO_2/ENR/PVC, the radicals increase the dye degradation rate.

Upon exposure to acid photoetching treatment, the oxirane ring in ENR-50 undergoes a ring-opening reaction [16]. HCl is a strong acid capable of donating a proton to the oxirane ring in ENR-50, resulting in the formation of an oxonium ion intermediate. This intermediate can undergo a ring-opening reaction, leading to the formation of a highly reactive carbocation intermediate. This carbocation can subsequently react with other molecules present in the system, including other ENR-50 molecules, PVC, or other suitable polymers, leading to the formation of crosslinked products.

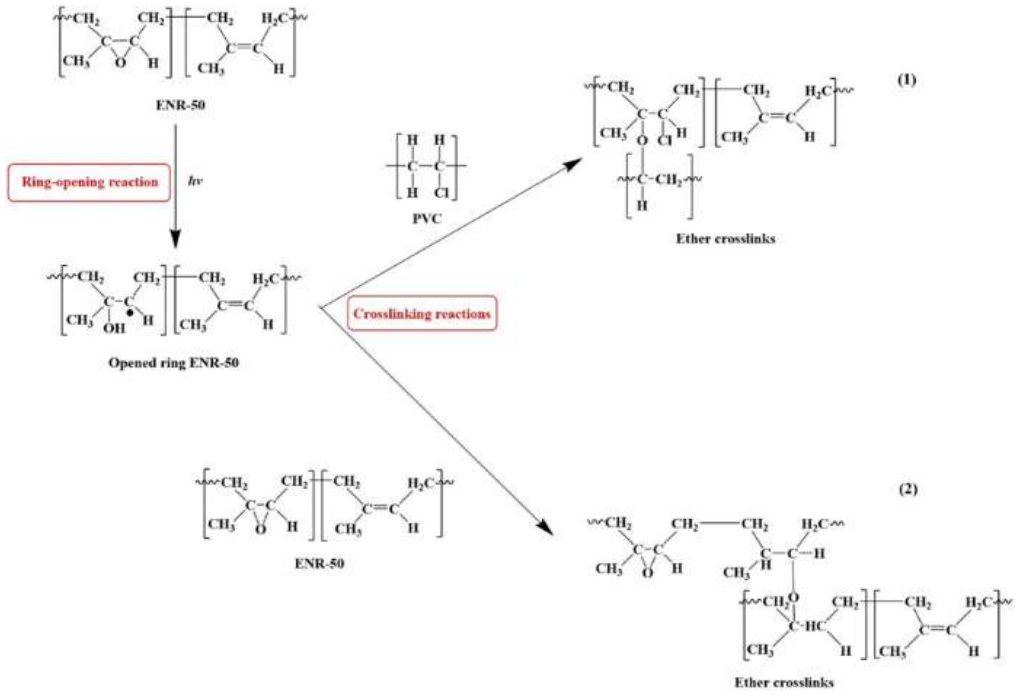

Figure 6. Probable reaction pathways for the normal photoetching process.

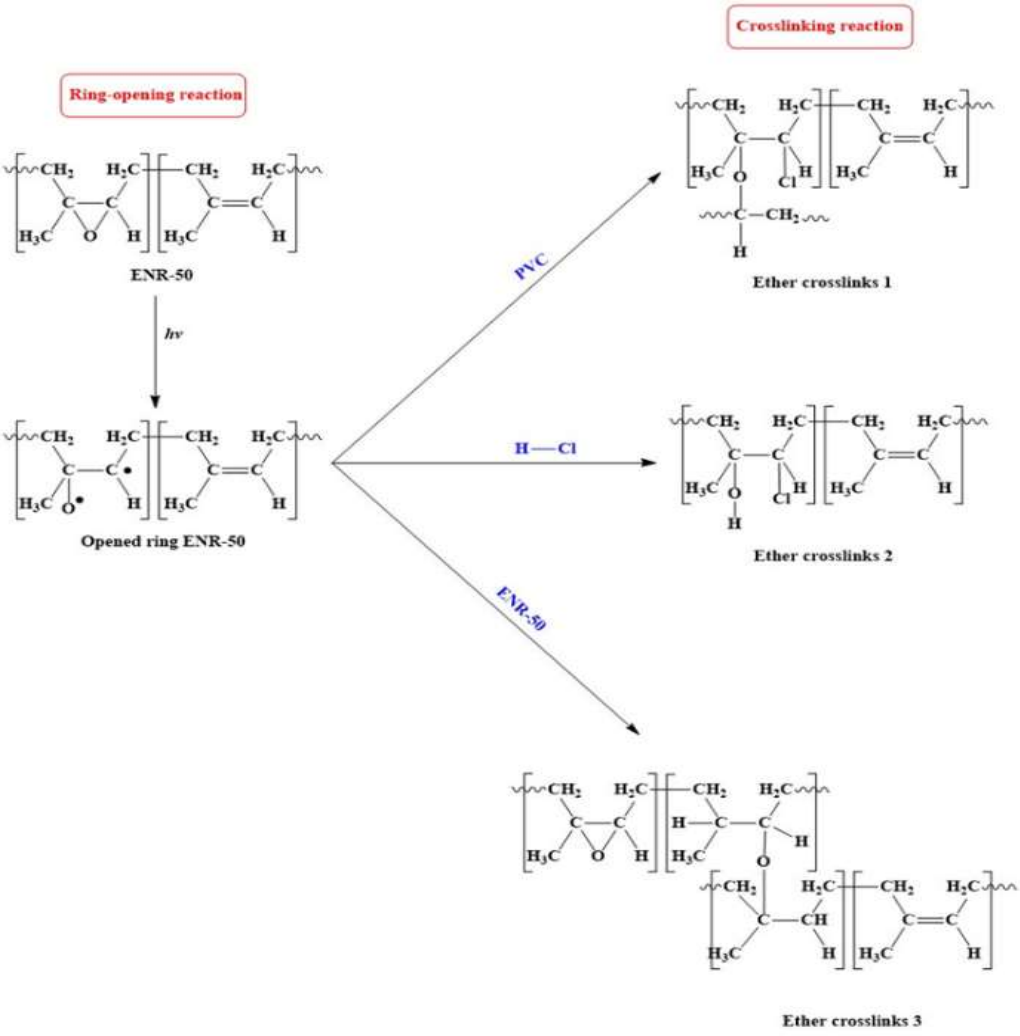

Figure 7. Possible reaction pathways during acid photoetching treatment of immobilized TiO_2/ENR/PVC.

The acid photoetching treatment of ENR-50 presents three possible reaction pathways, as demonstrated in Fig. 7. Firstly, the free radical may react with PVC or another suitable polymer, to form a crosslinked ENR-50-PVC or ENR-50-polymer product. Secondly, the free radical may react with hydrochloric acid molecules, forming a product in the presence of chloride (Cl). Finally, the oxirane ring in ENR-50 may open, resulting in the formation of a free radical that may react with another ENR-50 molecule. This type of product is known for its enhanced mechanical properties and adhesion to surfaces [5-6, 16, 39-40]. Consequently, a crosslinked ENR-50-PVC or ENR-50-polymer product is formed, incorporating both ENR-50 and the polymer. The opened ring of ENR-50 may also act as an electron injector, as the radicals generated have a high potential for degrading the model pollutant, as mentioned previously.

X-ray photoelectron spectroscopy (XPS) was performed to explore the results of the FTIR analysis in more detail and verify the suggested reaction mechanisms. The XPS spectrum depicted in Figure 6 elucidates the chemical states observed in both the NP and AP samples, showcasing the presence of TiO_2, ENR-50, and PVC elements through the representation of various states such as O1s, Ti2p, C1s, and Cl2p.

The binding energies of the peaks corresponding to the O1s, Ti2p, C1s, and Cl2p states for both samples were observed at 526, 454, 281, and 200 eV, respectively. However, these peaks displayed different intensities for each sample. The spectrum of the NP sample in Figure 8(a) revealed substantially higher intensities across all states in comparison to the AP sample. This observation implies the presence of elevated levels of TiO_2, ENR-50, and PVC elements in the NP sample.

Conversely, the AP sample demonstrated markedly low intensity signals for O1s, Ti2p, C1s, and notably Cl2p, as illustrated in Figure 8(b). This observed disparity may be attributed to the phenomenon of dehydrochlorination of PVC and the subsequent leaching of the polymer binder. These processes could potentially lead to a reduction in the immobilization of TiO_2 on the glass substrate during the acid photoetching treatment, thereby explaining the diminished intensities of certain peaks in the AP sample.

The deconvolution of each peak is displayed in Fig. 9. Upon further deconvolution of the peaks for C1s in both NP and AP samples, peaks at 286.8 and 284.5 eV were observed. These peaks corresponded to C-C and C-O bonds for epoxy, as indicated in Fig. 9(a-b). Additionally, the O1s core-level spectrum of NP and AP samples, depicted in Fig. 9(c-d), revealed the presence of oxygen species like C-O bonds related to the epoxy ring oxygen at 532.5 eV, and Ti-O bonds associated with the titanium dioxide oxygen at 529.8 eV.

In the AP sample (Fig. 9(d)), a decrease in the intensity of the Ti-O bond at 529.3 eV was observed, compared to the C-O bond. This reduction suggested a leaching of the polymer binder, leading to reduced TiO_2 immobility on the glass substrate. Furthermore, the Ti2p core-level spectrum (Fig. 9 (e-f)) exhibited the Ti2p½ and Ti2p3/2 states of both samples at 460 and 454 eV, respectively. The binding energies of these states showed slight shifts compared to pure TiO_2 as reported by Zhu et al. [50] at 464.1 and 458.4 eV, respectively. This shift could be due to the interactions between TiO_2 and the polymer binder (ENR-50/PVC).

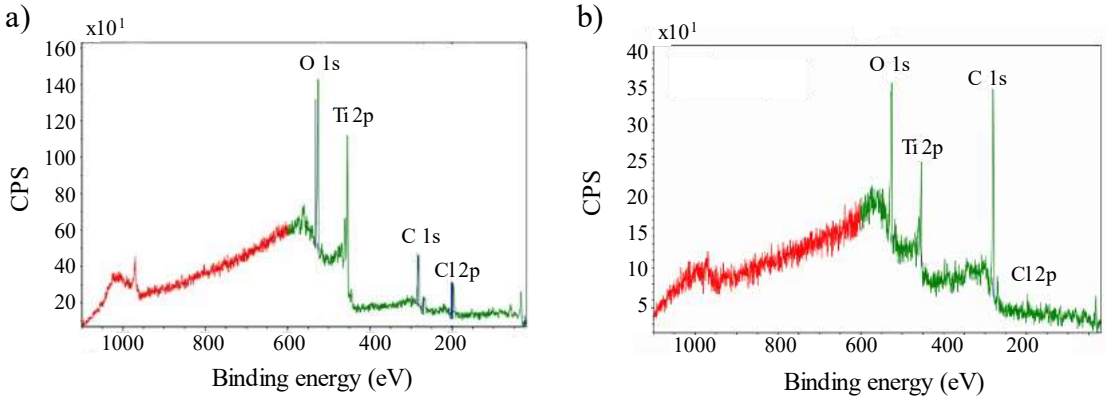

Figure 8. Wide XPS spectra of (a) NP, and (b) AP samples.

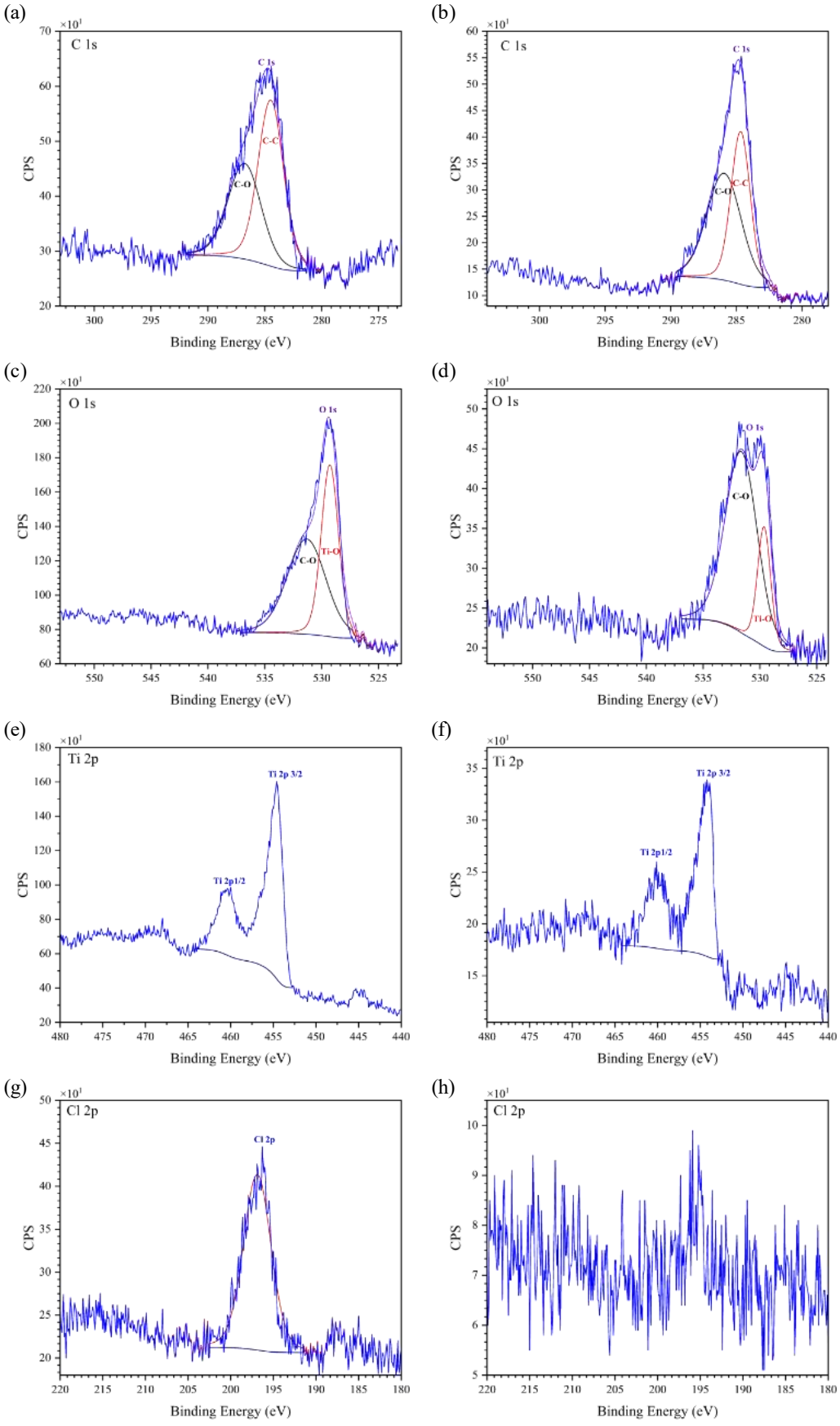

Figure 9. Deconvolution of XPS for each core-level spectrum for (a-b) C 1s, (c-d) O 1s, (e-f) Ti 2p and (g-h) Cl 2p states in the NP and AP samples, respectively.

Finally, Fig. 9(g-h) presents the Cl2p core-level spectrum, indicating the presence of chlorine in samples containing PVC. It was noted that the NP sample contained a higher amount of chlorine than the AP sample. The decrease in chlorine content in the AP sample confirmed the degradation of PVC by dehydrochlorination. These observations prove the potential crosslinking reaction between ENR-50 and both PVC and other ENR-50 molecules in the NP sample, and between ENR-50 molecules in the AP sample.

Photocatalytic Activity

Photoluminescence (PL) spectroscopy serves as a pivotal tool in the exploration of charge trapping, migration and transfer within semiconductor particles, along with the identification of electron-hole pair recombination [51-53]. Fig. 10 presents the analysis of PL spectra for WOP, NP, and AP during the 5th cycle, affirming photoexcitation. The analysis revealed that NP had a higher PL intensity in the sub-band range of 500-700 nm compared to AP and WOP, indicating a greater recombination of electron-hole pairs from the band to the sub-band of TiO_2. This can be attributed to the presence of surface oxygen vacancies and defects in the semiconductors [54].

On the other hand, AP had the lowest PL peak in the band-to-band range of 300-500 nm, indicating lower electron-hole recombination compared to NP and WOP. This implies that AP had the lowest electron-hole recombination value, leading to a sophisticated photocatalytic response in the 5th cycle. The presence of surface oxygen vacancies and defects in the semiconductors can affect electron-hole pair recombination and transfer, which ultimately affects the photocatalytic activity of a sample. The lower electron-hole recombination value of AP, which may be due to the presence of surface oxygen vacancies and defects, could explain its superior performance in the 5th cycle.

Overall, the PL spectra analysis highlights the significance of surface oxygen vacancies and defects in affecting electron-hole pair recombination and transfer, which ultimately influences the photocatalytic performance of the sample.

The photocatalytic degradation efficiency of immobilized TiO_2/ENR/PVC was evaluated using RR4 dye. Fig. 11 compares the rate constant values (k) for 18 cycles (1 cycle = 10 hours) under two conditions: normal photoetching (NP) and acid photoetching (AP). The WOP sample had a k value of 0.0162 min^{-1}, which was lower than that of the slurry P25 TiO_2 sample. This is due to the limited active sites on the immobilized TiO_2 compared to the slurry TiO_2. However, the treated immobilized TiO_2 (NP and AP samples) showed a higher k value than the WOP sample. This might be due to the increase in the active site surface area of TiO_2 after the photoetching treatment, as the ENR/PVC was slightly removed from the immobilized TiO_2, as mentioned by Nawi *et al* [39]. The photocatalytic performance of the NP and AP samples gradually increased up to the 12th cycle and achieved superior k values (0.1207 min^{-1} and 0.13 min^{-1} respectively) compared to the slurry P25 TiO_2.

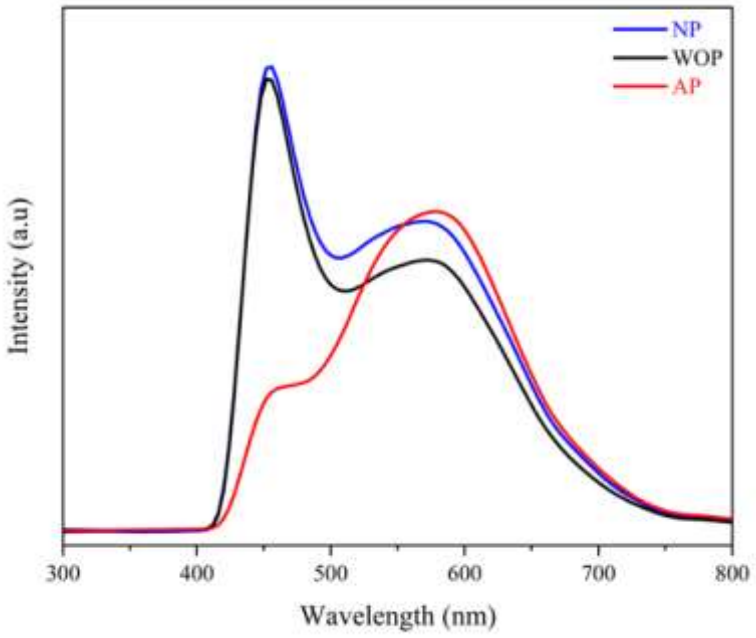

Figure 10. Photoluminescence (PL) spectroscopy of NP, AP and WOP after 50 hours.

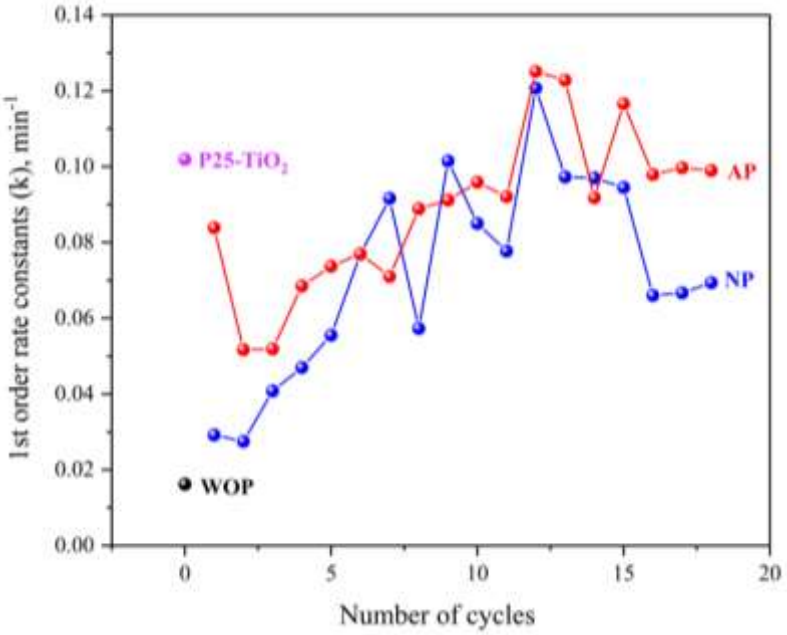

Figure 11. Pseudo first order rate constant (min^{-1}) vs cycles for the NP, DP and AP samples during photodegradation of RR4 dye.

The photoetching process leached ENR/PVC from the immobilized TiO_2, increasing its surface area and enhancing photocatalytic activity over multiple cycles, as demonstrated by previous researchers [39-40, 49]. Despite the leaching out of ENR/PVC from the immobilized TiO_2, the crosslinking reaction mentioned earlier may form products that improve the adhesiveness and durability of the immobilized sample. However, the photocatalytic performance of the NP and AP samples started to decrease from the 13^{th} cycle onwards due to the lower TiO_2 content, as TiO_2 may also have leached out from the immobilized system along with ENR/PVC.

Overall, although the AP sample exhibited a melted layer (see FESEM images in Fig. 2), it achieved excellent photocatalytic activity among all the samples, noticeably starting from the 13^{th} cycle of the recyclability experiment for RR4 dye photodegradation, as illustrated in Fig. 11. This may be due to other factors such as radical generation during ring-opening, by-products from the crosslinking reaction, and low electron hole recombination, which may cause the AP sample to have a dominant impact on the photodegradation of RR4 dye. These results indicate the significance of acid photoetching treatment on the immobilized TiO_2/ENR/PVC in the photodegradation of RR4 dye.

CONCLUSION

There were significant differences between the treated (photoetching and acid photoetching) and untreated samples, as a treated sample could enhance photocatalytic activity with its own unique characteristic effect. Under normal photoetching treatment, the NP sample showed an improved surface with high porosity. However, the acid photoetching treatment significantly enhanced the photocatalytic activity of immobilized TiO_2/ENR/PVC, although it had the lowest surface roughness and a melted layer surface structure. The superior photocatalytic activity shown by the AP sample may be due to the presence of HCl molecules and their reaction with the immobilized sample. Hence, instead of the TiO_2 active site surface area, the products generated from the open ring ENR-50 during acid photoetching treatment were identified as one of the factors that enhanced photocatalytic performance. This noteworthy discovery offers a potential approach to boosting the photocatalytic activity of other immobilized catalysts.

ACKNOWLEDGEMENTS

This work was supported by the Ministry of Higher Education, Malaysia (MOHE) [DPPD grant number: 600-TNCPI 5/3/DDN (09) (008/2023)]. The authors express their gratitude to Ms. Siti Sarina Binti Sulaiman for providing proofreading for this article. Furthermore, we would like to thank Universiti Malaysia Perlis (UniMAP) and Universiti Teknologi MARA (UiTM) for providing the necessary facilities.

REFERENCES

1. Berradi, M., Hsissou, R., Khudhair, M., Assouag, M., Cherkaoui, O., El Bachiri, A. & El Harfi, A.

(2019) Textile finishing dyes and their impact on aquatic environs. *Heliyon*, **5(11)**, e02711.

2. Saravanakumar, K., De Silva, S., Santosh, S. S., Sathiyaseelan, A., Ganeshalingam, A., Jamla, M. & Wang, M. H. (2022) Impact of industrial effluents on the environment and human health and their remediation using MOFs-based hybrid membrane filtration techniques. *Chemosphere*, 135593.

3. Zeshan, M., Bhatti, I. A., Mohsin, M., Iqbal, M., Amjed, N., Nisar, J. & Alomar, T. S. (2022) Remediation of pesticides using TiO_2 based photocatalytic strategies: A review. *Chemosphere*, 134525.

4. Shokri, A. & Sanavi Fard, M. (2022) A critical review in the features and application of photocatalysts in wastewater treatment. *Chemical Papers*, **76(9)**, 5309–5339.

5. Hamzah, S. R., Rosli, M. A., Natar, N. S., Ghani, N. I. A., Muhamad, N. A., Azami, M. S. & Nawawi, W. I. (2023) The Crosslinking and Porosity Surface Effects of Photoetching Process on Immobilized Polymer-Based Titanium Dioxide for the Decolorization of Anionic Dye. *Colorants*, **2(1)**, 73–89.

6. Rosli, M. A., Hamzah, S. R., Muhamad, N. A., Abdul, N. I., Ghani, N. S. M. N., Ab Aziz, S. I. & Nawawi, W. I. (2022) Acid Photo Etching Effect of Epoxidized Natural Rubber (ENR) and Polyvinyl Chloride (PVC) as Polymer Binder. *Malays. J. Chem.*, **24**, 228–239.

7. Natar, N. S., Ikhwan, S., Nazeri, N. S., Hamzah, S. R., Rosli, M. A., Ghani, N. I. & Nawawi, W. I. (2022) Preparation of water-base immobilized N doped TiO_2 using DSAT technique for photocatalytic degradation of methylene blue dye. *Materials Today: Proceedings*, **66**, 4036–4044.

8. Mendez-Arriaga, F., de la Calleja, E., Ruiz-Huerta, L., Caballero-Ruiz, A. & Almanza, R. (2019) TiO_2 3D structures for environmental purposes by additive manufacturing: Photoactivity test and reuse. *Materials Science in Semiconductor Processing*, **100**, 35–41.

9. Belver, C., Bedia, J., Gómez-Avilés, A., Peñas-Garzón, M. & Rodriguez, J. J. (2019) Semiconductor photocatalysis for water purification. In *Nanoscale materials in water purification, Elsevier*, 581–651.

10. Srikanth, B., Goutham, R., Narayan, R. B., Ramprasath, A., Gopinath, K. P. & Sankaranarayanan, A. R. (2017) Recent advancements in supporting materials for immobilised photocatalytic applications in waste water treatment. *Journal of Environmental Management*, **200**, 60–78.

11. Villalba-Rodríguez, A. M., Martínez-Zamudio, L. Y., Martínez, S. A. H., Rodríguez-Hernández, J. A., Melchor-Martínez, E. M., Flores-Contreras, E. A. & Parra-Saldívar, R. (2022) Nanomaterial Constructs for Catalytic Applications in Biomedicine: Nanobiocatalysts and Nanozymes. *Topics in Catalysis*, 1–16.

12. Zdarta, J., Jankowska, K., Bachosz, K., Degórska, O., Kaźmierczak, K., Nguyen, L. N. & Jesionowski, T. (2021) Enhanced wastewater treatment by immobilized enzymes. *Current Pollution Reports*, **7**, 167–179.

13. Yaashikaa, P. R., Devi, M. K. & Kumar, P. S. (2022) Advances in the application of immobilized enzyme for the remediation of hazardous pollutant: A review. *Chemosphere*, 134390.

14. Do, H. H., Tran, T. K. C., Ung, T. D. T., Dao, N. T., Nguyen, D. D., Trinh, T. H. & Tran, T. T. H. (2021) Controllable fabrication of photocatalytic TiO2 brookite thin film by 3D-printing approach for dyes decomposition. *Journal of Water Process Engineering*, **43**, 102319.

15. Shao, J. Y. & Zhong, Y. W. (2019) Stabilization of a cyclometalated ruthenium sensitizer on nanocrystalline TiO2 by an electrodeposited covalent layer. *Inorganic Chemistry*, **58(5)**, 3509–3517.

16. Romero-Arcos, M., Garnica-Romo, M. G. & Martínez-Flores, H. E. (2016) Electrochemical study and characterization of an amperometric biosensor based on the immobilization of laccase in a nanostructure of TiO2 synthesized by the sol-gel method. *Materials*, **9(7)**, 543.

17. Lang, J., Takahashi, K., Kubo, M. & Shimada, M. (2022) Ag-Doped TiO2 Composite Films Prepared Using Aerosol-Assisted, Plasma-Enhanced Chemical Vapor Deposition. *Catalysts*, **12(4)**, 365.

18. Chen, L. C., Ke, C. R., Hon, M. H. & Ting, J. M. (2015) Electrophoretic deposition of TiO2 coatings for use in all-plastic flexible dye-sensitized solar cells. *Surface and Coatings Technology*, **284**, 51–56.

19. Ghani, N. I. A., Rosli, M. A., Hamzah, S. R., Natar, N. S., Nazeri, N. S., Ab Aziz, S. I. & Ismail, W. I. N. W. (2022) Water-based Preparation of Immobilized Ag- doped TiO_2 Photocatalyst for Photocatalytic Degradation of RR4 Dye. *Science Letters*, **16(2)**, 24–39.

20. Chen, D., Cheng, Y., Zhou, N., Chen, P., Wang, Y., Li, K. & Ruan, R. (2020) Photocatalytic

degradation of organic pollutants using TiO2-based photocatalysts: A review. *Journal of Cleaner Production*, **268**, 121725.

21. Anandan, S. & Yoon, M. (2003) Photocatalytic activities of the nano-sized TiO_2- supported Y-zeolites. *Journal of Photochemistry and Photobiology C: Photochemistry Reviews*, **4(1)**, 5–18.

22. Adnan, M. A. M., Phoon, B. L. & Julkapli, N. M. (2020) Mitigation of pollutants by chitosan/metallic oxide photocatalyst: a review. *Journal of Cleaner Production*, **261**, 121190.

23. Pragada, S. C. & Thalla, A. K. (2021) Polymer-based immobilized Fe_2O_3– TiO_2/PVP catalyst preparation method and the degradation of triclosan in treated greywater effluent by solar photocatalysis. *Journal of Environmental Management*, **296**, 113305.

24. Wang, S., Xu, M., Peng, T., Zhang, C., Li, T., Hussain, I. & Tan, B. (2019) Porous hyper-crosslinked polymer-TiO_2-graphene composite photocatalysts for visible-light-driven CO2 conversion. *Nature communications*, **10(1)**, 676.

25. Fujishima, A. & Honda, K. (1972) Electrochemical photolysis of water at a semiconductor electrode. *Nature*, **238(5358)**, 37–38.

26. Lukhman, S., Natar, N., Ghani, N., Shukor, A., Nazeri, S., Ikhwan, S. & Izhan, W. (2021) Preparation of polyaniline/TiO_2 photovoltaic solar cell. *Science Letters (ScL)*, **15(2)**, 102–115.

27. Jaber, F. S. & Abduljalil, H. M. (2022) Preparation a Polymeric Composite PVA-TiO_2-Ag by Liquid Casting Method is Applicate it in Anti-bacteria Field. *NeuroQuantology*, **20(9)**, 36.

28. Ding, B., Kim, J., Kimura, E. & Shiratori, S. (2004) Layer-by-layer structured films of TiO_2 nanoparticles and poly (acrylic acid) on electro-spun nanofibres. *Nanotechnology*, **15(8)**, 913.

29. Anh, N. T. Q., Ngoc, H. M., Van Noi, N. & Van, N. H. (2023) Enhanced photocatalytic degradation of direct blue 71 dye using TiO_2-PAA-GO composite in aqueous solution. *Materials Research Express*, **10(5)**, 055503.

30. Najwa, N. A. K. Z., Juoi, J. M., Rosli, Z. M. & Moriga, T. (2020) Effect of PEG Loading on the Microstructure and Photocatalytic Activity of TiO_2 Film on Ceramic Tile. *Journal of Advanced Manufacturing Technology (JAMT)*, **14(2 (2))**.

31. Suganya, A., Shanmugavelayutham, G. & Rodríguez, C. S. (2017) Study on plasma pre-functionalized PVC film grafted with TiO_2/PVP to improve blood compatible and antibacterial properties. *Journal of Physics D: Applied Physics*, **50(14)**, 145402.

32. Farrokhi-Rad, M., Mohammadalipour, M. & Shahrabi, T. (2018) Electrophoretic deposition of titania nanostructured coatings for photo-degradation of methylene blue. *Ceramics International*, **44(9)**, 10716–10725.

33. Yang, L., Chen, C., Hu, Y., Wei, F., Cui, J., Zhao, Y. & Sun, D. (2020) Three- dimensional bacterial cellulose/polydopamine/TiO_2 nano-composite membrane with enhanced adsorption and photocatalytic degradation for dyes under ultraviolet-visible irradiation. *Journal of Colloid and Interface Science*, **562**, 21–28.

34. Bahrudin, N. N. (2022) Evaluation of degradation kinetic and photostability of immobilized TiO_2/activated carbon bilayer photocatalyst for phenol removal. *Applied Surface Science Advances*, **7**, 100208.

35. El Menoufy, H. A., Gomaa, S. K., Haroun, A. A., Farag, A. N., Shafei, M. S., Shetaia, Y. M. & Abd El Aal, R. A. (2022) Comparative studies of free and immobilized partially purified lipase from Aspergillus niger NRRL-599 produced from solid-state fermentation using gelatin-coated titanium nanoparticles and its application in textile industry. *Egyptian Pharmaceutical Journal*, **21(2)**, 143.

36. Singh, S., Mahalingam, H. & Singh, P. K. (2013) Polymer-supported titanium dioxide photocatalysts for environmental remediation: A review. *Applied Catalysis A: General*, **462**, 178–195.

37. Hong, H. J., Sarkar, S. K. & Lee, B. T. (2012) Formation of TiO_2 nano fibers on a micro-channeled Al_2O_3–ZrO_2/TiO_2 porous composite membrane for photocatalytic filtration. *Journal of the European Ceramic Society*, **32(3)**, 657–663.

38. Choudhary, R., Kumar, V. & Yadav, R. (2022) Nanotechnology in Packaging for Food Preservation. *Nanotechnology in Intelligent Food Packaging*, 313–341.

39. Nawi, M. A., Ngoh, Y. S. & Zain, S. M. (2012) Photoetching of Immobilized TiO_2-ENR50-PVC Composite for Improved Photocatalytic Activity. *International Journal of Photoenergy*, *2012*.

40. Ramlee, N. A., Ratnam, C. T., Alias, N. H. & Tengku Mohd, T. A. (2014) Effect of TiO_2 nano-fillers on mechanical properties of PVC/ENR/TiO_2 nanocomposites. *Advanced Materials Research*, **911**, 105–109.

41. Ramlee, N. A., Ratnam, C. T., Alias, N. H. & Abd Rahman, M. F. (2014) Dynamic mechanical and gel content properties of irradiated ENR/PVC blends with TiO_2 nanofillers. *International Journal of Science and Engineering*, **6(1)**, 24–30.

42. Hamzah, R., Bakar, M. A., Dahham, O. S., Zulkepli, N. N. & Dahham, S. S. (2016) A structural study of epoxidized natural rubber (ENR-50) ring opening under mild acidic condition. *Journal of Applied Polymer Science*, **133(43)**.

43. Li, Y., Du, J., Peng, S., Xie, D., Lu, G. & Li, S. (2008) Enhancement of photocatalytic activity of cadmium sulfide for hydrogen evolution by photoetching. *International Journal of Hydrogen Energy*, **33(8)**, 2007–2013.

44. Sadeghi, S. M., Vaezi, M., Kazemzadeh, A. & Jamjah, R. (2021) 3D networks of TiO_2 nanofibers fabricated by sol-gel/electrospinning/calcination combined method: Valuation of morphology and surface roughness parameters. *Materials Science and Engineering: B*, **271**, 115254.

45. Coto, M., Troughton, S. C., Knight, P., Joshi, R., Francis, R., Kumar, R. V. & Clyne, T. W. (2021) Optimization of the microstructure of TiO_2 photocatalytic surfaces created by Plasma Electrolytic Oxidation of titanium substrates. *Surface and Coatings Technology*, **411**, 127000.

46. Vittoni, C., Gatti, G., Paul, G., Mangano, E., Brandani, S., Bisio, C. & Marchese, L. (2019) Non-Porous versus Mesoporous Siliceous Materials for CO2 Capture. *ChemistryOpen*, **8(6)**, 719–727.

47. Fidelis, M. Z., de Paula, E., Abreu, E., Fuziki, M. E., dos Santos, O. A., Brackmann, R. & Lenzi, G. G. (2023) Nb_2O_5: Percentage Effect of T/H Phase and Evaluation of Catalytic Activity, a Preliminary Study. *Catalysis Research*, **3(3)**, 1–13.

48. Lee, G., Jin, M. J. & Lee, K. J. (2021) Structural effects of crack-free PMMA/Silane/$BaSO_4$-TiO_2 composite coating composed of bimodal particles via electrophoretic deposition on titanium substrate. *Surface and Coatings Technology*, **408**, 126788.

49. Ramlee, N. A., Ratnam, C. T., Rahman, S. A. & Samat, N. A. A. (2013) Incorporation of TiO_2 nanoparticles in PVC/ENR blends. In *2013 IEEE Business Engineering and Industrial Applications Colloquium (BEIAC)*, IEEE2013, 557–560, April 2013.

50. Zhu, X., Wen, G., Liu, H., Han, S., Chen, S., Kong, Q. & Feng, W. (2019) One-step hydrothermal synthesis and characterization of Cu-doped TiO2 nanoparticles/nanobucks/nanorods with enhanced photocatalytic performance under simulated solar light. *Journal of Materials Science: Materials in Electronics*, **30**, 13826–13834.

51. Li, F. B. & Li, X. Z. (2002) Photocatalytic properties of gold/gold ion-modified titanium dioxide for wastewater treatment. *Applied Catalysis A: General*, **228(1-2)**, 15–27.

52. Shanmugam, V. & Jeyaperumal, K. S. (2018) Investigations of visible light driven Sn and Cu doped ZnO hybrid nanoparticles for photocatalytic performance and antibacterial activity. *Applied Surface Science*, **449**, 617–630.

53. Gautam, N., Singh, K. B., Upadhyay, D. D. & Pandey, G. (2023) Structural and optical properties of silver supported α-Fe_2O_3 nano-composite fabricated by Saraca asoca leaf extract for the effective photo-degradation of cationic dye Azure B. *RSC Advances*, **13(33)**, 23181–23196.

54. Saha, A., Moya, A., Kahnt, A., Iglesias, D., Marchesan, S., Wannemacher, R. & Guldi, D. M. (2017) Interfacial charge transfer in functionalized multi-walled carbon nanotube@ TiO_2 nanofibres. *Nanoscale*, **9(23)**, 7911–7921.